JOURNAL OF PROPULSION AND POWER
Vol. 33, No. 1, January–February 2017

Effect of Azimuthally Nonuniform Heat Release on Longitudinal Combustion Instabilities

Lei Li* and Xiaofeng Sun†
Beijing University of Aeronautics and Astronautics, Beijing 100191, People's Republic of China
and
Christopher Lioi‡ and Vigor Yang§
Georgia Institute of Technology, Atlanta, Georgia 30327

DOI: 10.2514/1.B36055

Combustion instabilities arise from interactions between the acoustic field and unsteady heat release within a confined chamber. In the present study, a three-dimensional acoustic model is developed to explore the effect of azimuthally nonuniform distribution of heat release on longitudinal combustion instabilities. The governing equations are solved by means of a spectral collocation method with domain decomposition to accommodate the flow discontinuities across the flame. It is shown that the circumferential nonuniformity in heat release has only a marginal effect on instability frequency but may cause a potentially significant decrease in the growth rate. For some combinations of flow parameters, a high degree of heat-release asymmetry may qualitatively change the stability characteristics of the combustor, with a sign change of the growth rate. It is found that vorticity waves produced by the azimuthally nonuniform heat release may contribute damping to the thermoacoustic system.

Downloaded by GEORGIA INST OF TECHNOLOGY on March 24, 2017 | http://arc.aiaa.org | DOI: 10.2514/1.B36055

Nomenclature

C_p	=	constant pressure specific heat capacity
C_V	=	constant volume specific heat capacity
c	=	speed of sound
k	=	$\bar{T}_{02}/\bar{T}_{01}$, ratio of mean stagnation temperatures on either side of heat-release plane
N_x, N_r, N_θ	=	numbers of collocation points in axial, radial, and circumferential directions
n	=	interaction index (gain) for $n-\tau$ combustion response model
$\bar{\dot{Q}}$	=	time-averaged rate of heat release per unit area due to combustion
$\dot{Q}'$	=	fluctuating rate of heat release per unit area due to combustion
R_p, R_u	=	complex pressure and velocity-coupled combustion response functions
x, r, θ	=	axial, radial, and circumferential coordinate variables
α	=	growth rate (imaginary part of Ω)
σ	=	amplitude of sinusoidal circumferential distribution of combustion response parameters
τ	=	time delay for $n-\tau$ combustion response model
Ω	=	complex eigenfrequency
ω	=	angular frequency (real part of Ω)

I. Introduction

COMBUSTION instabilities present a major challenge to the development and operation of many propulsion systems, including solid rocket motors [1,2], liquid rocket engines [3–5], ramjets and scramjets [6–9], and gas turbine combustors [10,11]. They result from the energy exchange between the acoustic field and transient combustion response and manifest as finite-amplitude flow oscillations. The ensuing pressure excursions are implicated in a multitude of deleterious effects, including reduced operating lifetime of engine components and, in extreme cases, catastrophic failure, due to vibration and enhanced heat transfer to engine hardware. It is of paramount importance to establish thorough understanding of the physiochemical mechanisms responsible for and operating conditions conducive to the initiation and sustainment of combustion instabilities. Recent research, comprising robust analytical, experimental, and numerical studies, has shed light on some aspects of these mechanisms, but additional work is needed, especially on problems involving complex geometries and flowfields.

Generally, combustion instabilities are initiated when a random perturbation in intrinsic combustor noise is amplified by linear mechanisms. The growth of oscillations is limited by nonlinear processes, and eventually the unsteady pressure field saturates at some limit cycle amplitude. Oscillations typically occur at one or more of the natural acoustic frequencies of the combustor, which suggests that the unsteady pressure field may be constructed as a synthesis of classical mode shapes. Culick [12,13] and Culick and Yang [14,15] used a Galerkin approach based on this principle to map stability boundaries and determine the temporal evolution of modal amplitudes for a variety of model combustors. It has also been thought possible to excite a linearly stable system to limit-cycle oscillations by a finite-amplitude pressure pulse, a phenomenon known as pulse-triggered instability. This problem has been quantitatively addressed in the context of solid rocket motors [16,17]. Yang et al. [16] found that nonlinear gas dynamics alone does not provide a mechanism for triggering a finite disturbance to limit cycles in a linearly stable system. In order for triggering to occur, nonlinear combustion response must be present. To this end, Wicker et al. [17] extended the work of Yang et al. [16] to study the effect of several functional forms of combustion response and found that only certain forms allowed for triggering to take place. In particular, it is not possible to trigger a finite disturbance to a stable limit cycle if the combustion response is proportional to any quadratic function of acoustic pressure and velocity. Triggering, however, may occur if the response is proportional to the magnitude of the acoustic velocity. More recently, Flandro et al. [18] explored the existence of triggering by reference to a large body of experimental data for solid-propellant rocket motors. They suggested that many motors thought to exhibit triggering were in fact intrinsically linearly unstable but that the instabilities had vanishingly small growth rates. Regardless, it is evident that the problem of linear stability is the more fundamental issue and therefore is the focus of this study.

Received 25 October 2015; revision received 12 April 2016; accepted for publication 13 April 2016; published online 26 August 2016. Copyright © 2016 by the American Institute of Aeronautics and Astronautics, Inc. All rights reserved. Copies of this paper may be made for personal and internal use, on condition that the copier pay the per-copy fee to the Copyright Clearance Center (CCC). All requests for copying and permission to reprint should be submitted to CCC at www.copyright.com; employ the ISSN 0748-4658 (print) or 1533-3876 (online) to initiate your request.

*Postdoctor, School of Jet Propulsion; currently Lecturer in Shanghai Jiao Tong University; Lesanstone@126.com.
†Professor, School of Jet propulsion; Sunxf@buaa.edu.cn (Corresponding Author).
‡Graduate Student; clioi3@gatech.edu.
§William R. T. Professor and Chair; vigor.yang@aerospace.gatech.edu.

Downloaded by GEORGIA INST OF TECHNOLOGY on March 24, 2017 | http://arc.aiaa.org | DOI: 10.2514/1.B36055

According to Rayleigh's criterion [19,20], fluctuating heat release will drive acoustic oscillations, provided that the magnitude of the relative phase between heat release and unsteady pressure is less than 90 deg. If the energy transferred to the acoustic field is greater than the energy radiated or convected out of the domain and dissipated within it by viscous processes, then the amplitude of oscillations will grow, and the system is deemed linearly unstable. The fluctuating heat release, in turn, depends on acoustic and flow perturbations. Several driving mechanisms, including harmonic acoustic forcing, equivalence-ratio oscillations, fuel flow-rate oscillations, unsteady mixing and phase-change processes, vortex shedding, and flame front dynamics have been identified as potential contributors to oscillatory heat release [11].

The present work deals with the interaction among acoustic, vortical, and entropy disturbances and their collective coupling with unsteady heat release. Vortical and entropy disturbances are often excluded from combustion instability analyses for the sake of analytical tractability, but this omits critical physics. For example, entropy disturbances produced by unsteady combustion will generate upstream propagating acoustic waves upon acceleration through a field of nonuniform mean velocity such as a nozzle [21,22]. This phenomenon is potentially problematic because the resulting acoustic waves may further perturb the combustion process and thus cause an otherwise stable system to become unstable. Studies demonstrating the critical nature of this coupling can be found in [23–25]. Additionally, even assuming the acoustic medium to be free of inhomogeneities such as mean temperature gradients, acoustic and entropy disturbances are known to couple in the presence of nonuniform mean flow. Vortical disturbances may also have a significant effect on the stability of a combustor in some cases. The recent investigation by Li and Sun [26] of an annular combustor with a compact flame indicated that, for purely azimuthal instabilities, the generation of vorticity waves accounts for significant acoustic damping.

Another aspect of the instability problem that does not seem to have received much systematic treatment in the literature is the azimuthal distribution of heat release. In real systems, perfect axisymmetry is not guaranteed. Annular gas turbines, liquid rocket engines, and other systems in which multiple discrete flame stabilization sites are distributed azimuthally may experience nonuniformities in the distributions of flow parameters and heat release either by design or through operational failure. For example, in many combustors, the spatial distribution of fuel injection is nonuniform, and this leads to azimuthal variations in flame geometry (and therefore heat-release rate). Alternatively, when all injection sites are nominally identical, local flame burnout during operation means that the heat release can no longer be even approximately axisymmetric. Circumferential variations in heat release and temperature may also arise in single-flame combustors in which the flame exhibits a high degree of asymmetry due to, for example, asymmetric mean flow [27]. The effects of such nonuniformities are not immediately obvious but might include preferential acoustic mode excitation or damping and thus may have an impact on the operational safety margins of the device. Based on these considerations, an examination of the effects of azimuthal nonuniformities of the flowfield and heat release represents a practical extension of existing theories. An earlier investigation of the authors [28] considered the effects of a nonuniform azimuthal distribution on purely longitudinal acoustic motions in a model combustor. The flame in that study, however, was not assumed to be acoustically compact in the axial direction. A clear study of the coupling between the circumferential distribution of heat release and the generation of entropy and vorticity waves was thus rendered difficult.

The key purpose of this work is to systematically investigate the effects on acoustic stability of 1) coupling with vortical and entropic motions, and 2) circumferential nonuniformities in heat release. A theoretical model based on the inviscid equations of motion is developed and used to study the stability characteristics of a cylindrical combustor with a planar flame. The formulation for the oscillatory flowfield is solved by means of a spectral collocation method, in which the solution is expressed as a weighted superposition of basis functions appropriate to the geometry and boundary conditions. The result is required to satisfy the differential equations exactly at certain collocation points within the computational domain. A domain decomposition technique is used to accommodate the discontinuities in flow variables across the flame. Because the flame dynamics are not explicitly computed as part of the study, a velocity-coupled combustion response function is employed as a specific example to close the formulation for flow oscillations and unsteady heat release.

II. Theoretical Model

Figure 1 shows the physical configuration of concern: a cylindrical duct containing a planar flame separating the upstream and downstream regions.

The formulation begins with the conservation equations of mass, momentum, and energy for the gases within the chamber. In the absence of viscous and external forces, they take the following forms:

$$\frac{\partial \rho}{\partial t} + \nabla \cdot (\rho \boldsymbol{u}) = 0 \tag{1}$$

$$\rho \frac{\mathrm{d}\boldsymbol{u}}{\mathrm{d}t} + \nabla p = 0 \tag{2}$$

$$\rho T \frac{\mathrm{d}s}{\mathrm{d}t} = q(\boldsymbol{r}, t) \tag{3}$$

where ρ is the density, p is the pressure, $\boldsymbol{u}$ is the velocity, s is the entropy, T is the temperature, and q is the heat release per unit volume. For a perfect gas,

$$p = R_g \rho T \tag{4}$$

where $R_g = C_p - C_v$ is the gas constant, and C_p and C_v are specific heats at constant pressure and volume, respectively. The total differential of density is

$$\mathrm{d}\rho = \left.\frac{\partial \rho}{\partial p}\right|_s \mathrm{d}p + \left.\frac{\partial \rho}{\partial s}\right|_p \mathrm{d}s \tag{5}$$

With the application of Eq. (4), this can be written as

$$\mathrm{d}s = \frac{C_p}{\rho c^2}\,\mathrm{d}p - \frac{C_p}{\rho}\,\mathrm{d}\rho \tag{6}$$

where c is the speed of sound. Substitution of Eq. (6) into Eq. (3) results in

$$\frac{\mathrm{d}p}{\mathrm{d}t} - c^2 \frac{\mathrm{d}\rho}{\mathrm{d}t} = (\gamma - 1) q(\boldsymbol{r}, t) \tag{7}$$

where $\gamma = C_p/C_v$ is the ratio of specific heats. Each variable can be decomposed into a mean (denoted by overbar –) and a small perturbation quantity, i.e.,

$$\begin{aligned} \boldsymbol{u}(\boldsymbol{r}, t) &= \bar{\boldsymbol{u}}(\boldsymbol{r}) + \boldsymbol{u}'(\boldsymbol{r}, t) \\ \rho(\boldsymbol{r}, t) &= \bar{\rho}(\boldsymbol{r}) + \rho'(\boldsymbol{r}, t) \\ p(\boldsymbol{r}, t) &= \bar{p}(\boldsymbol{r}) + p'(\boldsymbol{r}, t) \\ \hat{q}(r, t) &= \bar{q}(\boldsymbol{r}) + q'(\boldsymbol{r}, t) \end{aligned} \tag{8}$$

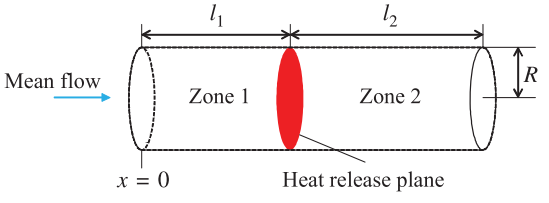

Fig. 1 Chamber geometry for model duct, including planar flame.

Downloaded by GEORGIA INST OF TECHNOLOGY on March 24, 2017 | http://arc.aiaa.org | DOI: 10.2514/1.B36055

Hence, from Eqs. (1), (2), and (7), the linearized equations for the perturbations are

$$\frac{\partial \rho'}{\partial t} + \nabla \cdot (\bar{\rho}\boldsymbol{u}') + \nabla \cdot (\rho'\bar{\boldsymbol{u}}) = 0 \tag{9}$$

$$\bar{\rho}\frac{\partial \boldsymbol{u}'}{\partial t} + \rho'\frac{\partial \bar{\boldsymbol{u}}}{\partial t} + \bar{\rho}\bar{\boldsymbol{u}}\cdot\nabla\boldsymbol{u}' + \bar{\rho}\boldsymbol{u}'\cdot\nabla\bar{\boldsymbol{u}} + \rho'\bar{\boldsymbol{u}}\cdot\nabla\bar{\boldsymbol{u}} + \nabla p' = 0 \tag{10}$$

$$\frac{\partial p'}{\partial t} + \bar{\boldsymbol{u}}\cdot\nabla p' + \boldsymbol{u}'\cdot\nabla\bar{p} - \bar{c}^2\frac{\partial \rho'}{\partial t} - \frac{\gamma}{\bar{\rho}}p'\frac{\partial \bar{\rho}}{\partial t} + \frac{\bar{c}^2}{\bar{\rho}}\rho'\frac{\partial \bar{\rho}}{\partial t} - \bar{c}^2\bar{\boldsymbol{u}}\cdot\nabla\rho' - \bar{c}^2\boldsymbol{u}'\cdot\nabla\bar{\rho} - \frac{\gamma}{\bar{\rho}}p'\bar{\boldsymbol{u}}\cdot\nabla\bar{\rho} + \frac{\bar{c}^2}{\bar{\rho}}\rho'\bar{\boldsymbol{u}}\cdot\nabla\bar{\rho} = (\gamma-1)q \tag{11}$$

We assume the perturbations to be time harmonic, so that

$$\begin{aligned} \rho'(\boldsymbol{r},t) &= \hat{\rho}(\boldsymbol{r})e^{-i\Omega t} \\ p'(\boldsymbol{r},t) &= \hat{p}(\boldsymbol{r})e^{-i\Omega t} \\ \boldsymbol{u}'(\boldsymbol{r},t) &= \hat{\boldsymbol{u}}(\boldsymbol{r})e^{-i\Omega t} \\ q'(\boldsymbol{r},t) &= \hat{q}(\boldsymbol{r})e^{-i\Omega t} \end{aligned} \tag{12}$$

Here, the overhat denotes a complex function of spatial coordinates. The characteristic modal frequency Ω is also complex:

$$\Omega = \omega + i\alpha \tag{13}$$

where i is the imaginary unit. The real part ω represents the radial frequency of oscillation, and the imaginary part α is the growth constant. Assuming that the mean quantities are steady with time, Eqs. (9–11) reduce to

$$-i\Omega\hat{\rho} + \nabla\cdot(\hat{\rho}\,\bar{\boldsymbol{u}}) + \nabla\cdot(\bar{\rho}\,\hat{\boldsymbol{u}}) = 0 \tag{14}$$

$$\hat{\rho}\,\bar{\boldsymbol{u}}\cdot\nabla\bar{\boldsymbol{u}} - i\Omega\bar{\rho}\,\hat{\boldsymbol{u}} + \bar{\rho}\,\bar{\boldsymbol{u}}\cdot\nabla\hat{\boldsymbol{u}} + \bar{\rho}\,\hat{\boldsymbol{u}}\cdot\nabla\bar{\boldsymbol{u}} + \nabla\hat{p} = 0 \tag{15}$$

$$\left(i\Omega\bar{c}^2 + \frac{\bar{c}^2}{\bar{\rho}}\bar{\boldsymbol{u}}\cdot\nabla\bar{\rho}\right)\hat{\rho} - \bar{c}^2\bar{\boldsymbol{u}}\cdot\nabla\hat{\rho} + \hat{\boldsymbol{u}}\cdot\nabla\bar{p} - \bar{c}^2\hat{\boldsymbol{u}}\cdot\nabla\bar{\rho} + \left(-i\Omega - \frac{\gamma}{\bar{\rho}}\bar{\boldsymbol{u}}\cdot\nabla\bar{\rho}\right)\hat{p} + \bar{\boldsymbol{u}}\cdot\nabla\hat{p} = (\gamma-1)\hat{q} \tag{16}$$

Expansion of the equations in cylindrical coordinates produces

$$A_1\hat{\rho} + A_2\frac{\partial\hat{\rho}}{\partial x} + A_3\frac{\partial\hat{u}_r}{\partial r} + A_4\frac{\partial\hat{u}_\theta}{\partial\theta} + A_5\frac{\partial\hat{u}_x}{\partial x} + A_6\hat{u}_r + A_7\hat{u}_\theta + A_8\hat{u}_x = 0 \tag{17}$$

$$B_1\hat{u}_r + B_2\frac{\partial\hat{u}_r}{\partial x} + B_3\frac{\partial\hat{p}}{\partial r} = 0 \tag{18}$$

$$C_1\hat{u}_\theta + C_2\frac{\partial\hat{u}_\theta}{\partial x} + C_3\frac{\partial\hat{p}}{\partial\theta} = 0 \tag{19}$$

$$D_1\hat{\rho} + D_2\hat{u}_x + D_3\frac{\partial\hat{u}_x}{\partial x} + D_4\hat{u}_r + D_5\hat{u}_\theta + D_6\frac{\partial\hat{p}}{\partial x} = 0 \tag{20}$$

$$E_1\hat{\rho} + E_2\frac{\partial\hat{\rho}}{\partial x} + E_3\hat{u}_r + E_4\hat{u}_\theta + E_5\hat{u}_x + E_6\hat{p} + E_7\frac{\partial\hat{p}}{\partial x} = (\gamma-1)\hat{q} \tag{21}$$

where u_x, u_r, and u_θ are the velocity in the axial, radial, and circumferential directions, respectively. The coefficients A, B, C, D, and E are functions of the mean flow variables given in the Appendix. Equations (17–21) are the basic equations governing the stability problem. For simplicity, in the present work, we consider a purely axial mean flow, whose spatial variation in the axial direction is included. The formulation outlined previously, however, is capable of incorporating spatially varying radial and circumferential mean velocities in a straightforward manner.

A. Spectral Collocation Discretization

Spectral methods have been widely used in solving eigenvalue problems for flow stabilities because of their fast convergence and high accuracy. Collocation methods in particular, such as the one employed here, tend to be more robust and adaptive than Galerkin-type methods. To discretize Eqs. (17–21), the Fourier method is employed for the periodic circumferential direction. The main drawback of this method is the presence of Gibbs oscillations in nonperiodic problems. Hence, the radial and axial directions are discretized using the Chebyshev expansion.

For Fourier methods, the collocation points are defined by

$$x_i = \frac{2\pi i}{N}, \qquad i = 0, \ldots, N \tag{22}$$

An arbitrary smooth function $v(x)$ can then be approximated by the discrete Fourier expansion

$$v_K(x) = \sum_{k=-K}^{K} \widehat{v}_k e^{ikx} \tag{23}$$

where $\widehat{v}_k$ are the unknown coefficients for $k = -K, \ldots, K$. The pth derivative at the collocation point can be derived as a function of the grid values $v_k(x_j)$:

$$v_K^{(p)}(x_i) = \sum_{j=1}^{N} e_{i,j}^{(p)} v_K(x_j), \qquad i = 1, \ldots, N \tag{24}$$

Here, $e_{i,j}^{(p)}$ is the pth Fourier derivative matrix given by Peyret.

For Chebyshev methods, collocation points are defined as Gauss–Lobatto points:

$$x_i = \cos\left(\frac{\pi i}{k}\right), \qquad i = 0, \ldots, k \tag{25}$$

The Chebyshev approximation of the function $v(x)$ defined for x in the range $[-1, 1]$ is

$$v_N(x) = \sum_{k=0}^{N} \widehat{v}_k T_k(x) \tag{26}$$

where $\hat{v}_k$ are the expansion coefficients, and $T_k(x)$ is the Chebyshev polynomial of degree k defined for x in the range $[-1, 1]$:

$$T_k(x) = \cos(k\cos^{-1}x), \qquad k = 0, 1, 2, \ldots \tag{27}$$

The pth derivative at the collocation points can be derived as a function of the grid values:

$$v_N^{(p)}(x_i) = \sum_{j=0}^{N} d_{i,j}^{(p)} v_N(x_j), \qquad i = 0, \ldots, N \tag{28}$$

where $d_{i,j}^{(p)}$ is the pth Chebyshev derivative matrix, also given by Peyret.

In Eqs. (17–21), the unknowns ρ, u_x, u_r, u_θ, and p are discretized by Fourier methods in the circumferential direction and Chebyshev methods in the axial and radial directions:

$$\chi(x, r, \theta) = \sum_{i=0}^{N_x} \sum_{j=0}^{N_r} \sum_{k=1}^{N_\theta} F_{ijk} T_i(x) T_j(r) e^{ik\theta} \tag{29}$$

where χ represents unknowns ρ, u_x, u_r, u_θ, and p, and F_{ijk} denotes the unknown coefficients. According to Eqs. (24) and (28),

$$\left.\frac{\partial \chi}{\partial x}\right|_{i,j,k} = \chi_x^1(x_i, r_j, \theta_k) = \sum_{m=0}^{N_x} d_{i,m}^1 \chi(x_m, r_j, \theta_k) \tag{30}$$

$$\left.\frac{\partial \chi}{\partial r}\right|_{i,j,k} = \chi_r^1(x_i, r_j, \theta_k) = \sum_{n=0}^{N_r} d_{j,n}^1 \chi(x_i, r_n, \theta_k) \tag{31}$$

$$\left.\frac{\partial \chi}{\partial \theta}\right|_{i,j,k} = \chi_\theta^1(x_i, r_j, \theta_k) = \sum_{p=1}^{N_\theta} e_{k,p}^1 \chi(x_i, r_j, \theta_p) \tag{32}$$

where $i = 0, \ldots, N_x$, $j = 0, \ldots, N_r$, and $k = 0, \ldots, N_\theta$.

B. Domain Decomposition Method

The source term $\hat{q}$ in Eq. (21) denotes unsteady heat release. We model this term as linearly dependent on the unsteady pressure and velocity to close the formulation:

$$\hat{q} = R_p \hat{p} + R_u \hat{u}_x \tag{33}$$

where R_p and R_u are complex pressure- and velocity-coupled combustion response functions, respectively. Equation (21) then becomes

$$E_1 \hat{\rho} + E_2 \frac{\partial \hat{\rho}}{\partial x} + E_3 \hat{u}_r + E_4 \hat{u}_\theta + E_5 \hat{u}_x + E_6 \hat{p} + E_7 \frac{\partial \hat{p}}{\partial x} = 0 \tag{34}$$

The coefficients E_1, E_2, E_3, E_4, and E_7 remain identical to those appearing in Eq. (21), whereas E_5 and E_6 now become

$$E_5 = \begin{cases} \frac{1}{\bar{c}^2}\frac{\partial \bar{p}}{\partial x} - \frac{\partial \bar{\rho}}{\partial x}, & x \neq x_0 \\ \frac{1}{\bar{c}^2}\frac{\partial \bar{p}}{\partial x} - \frac{\partial \bar{\rho}}{\partial x} - \frac{1}{\bar{c}^2} R_p, & x = x_0 \end{cases} \tag{35}$$

$$E_6 = \begin{cases} -i\Omega \frac{1}{\bar{c}^2} - \frac{\gamma \bar{u}_x}{\bar{c}^2 \bar{\rho}}\frac{\partial \bar{\rho}}{\partial x}, & x \neq x_0 \\ -i\Omega \frac{1}{\bar{c}^2} - \frac{\gamma \bar{u}_x}{\bar{c}^2 \bar{\rho}}\frac{\partial \bar{\rho}}{\partial x} - \bar{c}^2 R_p, & x = x_0 \end{cases} \tag{36}$$

where use has been made of the sifting property of the Dirac delta function. Equation (34) is discontinuous at the flame front $x = x_0$, with abrupt changes of the flow properties. The coefficients in Eqs. (17–20) are also discontinuous across the flame. A domain decomposition method is applied, in which $x < x_0$ is specified as one domain, and $x > x_0$ is another. In this method, the solutions are taken to be continuous in each subdomain, and continuity conditions are imposed to match the solutions at the flame interface.

Figure 2 depicts a small region dx containing the heat-release plane. Integration of the mass conservation equation over the control volume in the limit of d$x \to 0$ results in

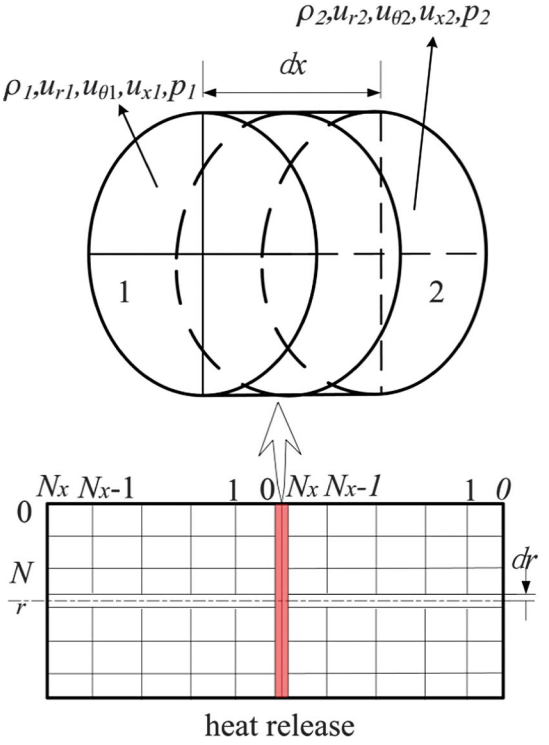

Fig. 2 Domain decomposition of model geometry.

$$\oint_s \rho \boldsymbol{u} \cdot \mathrm{d}\boldsymbol{s} = 0 \tag{37}$$

Equation (37) is linearized to yield

$$\bar{\rho}_1 u'_{xA} + \bar{u}_{x1} \rho'_A = \bar{\rho}_2 u'_{xB} + \bar{u}_{x2} \rho'_B \tag{38}$$

Subscripts 1 and 2 indicate parameters in the upstream and downstream regions, respectively. Subscripts A and B refer specifically to quantities on the heat-release plane in these two respective regions.

Integration of the momentum conservation equation in the control volume in the limit of d$x \to 0$ leads to

$$\oint_s \rho \boldsymbol{u}\boldsymbol{u} \cdot \mathrm{d}\boldsymbol{s} + \oint_s p \, \mathrm{d}\boldsymbol{s} = 0 \tag{39}$$

After linearization, we have

$$p'_A + \rho'_A \bar{u}_{x1}^2 + 2\bar{\rho}_1 \bar{u}_{x1} u'_{xA} = p'_B + \rho'_B \bar{u}_{x2}^2 + 2\bar{\rho}_2 \bar{u}_{x2} u'_{xB} \tag{40}$$

$$\bar{\rho}_1 \bar{u}_{x1} u'_{rA} = \bar{\rho}_2 \bar{u}_{x2} u'_{rB} \tag{41}$$

$$\bar{\rho}_1 \bar{u}_{x1} u'_{\theta A} = \bar{\rho}_2 \bar{u}_{x2} u'_{\theta B} \tag{42}$$

where the subscripts have the same interpretation as before. The energy conservation equation is written as

$$\delta \dot{Q} + \oint_s \left(e + \frac{p}{\rho} + \frac{U^2}{2} \right) \rho \boldsymbol{u} \cdot \mathrm{d}\boldsymbol{s} = 0 \tag{43}$$

where e is the internal energy, U is the velocity magnitude, and $\delta \dot{Q}$ is the heat release within the control volume. Linearization of Eq. (43) leads to

Downloaded by GEORGIA INST OF TECHNOLOGY on March 24, 2017 | http://arc.aiaa.org | DOI: 10.2514/1.B36055

$$\dot{Q}' + (C_p\bar{T}_{01}\bar{\rho}_1 + \bar{\rho}_1\bar{u}_{x1}^2)u'_{xA} + (C_p\bar{T}_{01}\bar{u}_{x1} - C_p\bar{T}_1\bar{u}_{x1})\rho'_A + \frac{C_p\bar{u}_{x1}}{Rg}p'_A = (C_p\bar{T}_{02}\bar{\rho}_2 + \bar{\rho}_2\bar{u}_{x2}^2)u'_{xB} + (C_p\bar{T}_{02}\bar{u}_{x2} - C_p\bar{T}_2\bar{u}_{x2})\rho'_B + \frac{C_p\bar{u}_{x2}}{Rg}p'_B \tag{44}$$

where

$$\dot{Q}' = \int_0^L \hat{q}(x)e^{i\Omega t}\,\mathrm{d}x$$

is the unsteady heat release per unit flame area, to be distinguished from q', the unsteady heat release per unit volume; T_{01} and T_{02} are the stagnation temperatures in the left and right domains, respectively. The stagnation temperatures have the form $T_0 = T + U^2/(2C_p)$. Introducing pressure- and velocity-coupled response functions given in Eq. (33), Eq. (44) becomes

$$(R_v + C_p\bar{T}_{01}\bar{\rho}_1 + \bar{\rho}_1\bar{u}_{x1}^2)u'_{xA} + (C_p\bar{T}_{01}\bar{u}_{x1} - C_p\bar{T}_1\bar{u}_{x1})\rho'_A + \left(R_p + \frac{C_p\bar{u}_{x1}}{Rg}\right)p'_A = (C_p\bar{T}_{02}\bar{\rho}_2 + \bar{\rho}_2\bar{u}_{x2}^2)u'_{xB} + (C_p\bar{T}_{02}\bar{u}_{x2} - C_p\bar{T}_2\bar{u}_{x2})\rho'_B + \frac{C_p\bar{u}_{x2}}{Rg}p'_B \tag{45}$$

Equations (38), (40–42), and (45) constitute jump conditions across the flame.

C. Boundary Conditions

Taking the chamber walls to be rigid, and neglecting both the mean flow and acoustic boundary layers, we have the boundary condition

$$\left.\frac{\partial p'}{\partial r}\right|_{r=R_o} = 0 \tag{46}$$

where R_o is the duct radius. This is equivalent to specifying a zero radial component of acoustic velocity at $r = R_o$ In cylindrical coordinates, this method leads to a coordinate singularity at $r = 0$. Several studies have discussed methods of circumventing this difficulty. We use the mapping technique introduced by Heinrichs [29].

Boundary conditions are also required at the inflow and outflow planes of the duct. At the inlet, no vorticity or entropy waves are present. Thus,

$$\frac{1}{R}\frac{\partial u'_{x1}}{\partial\theta} - \left.\frac{\partial u'_{\theta 1}}{\partial x}\right|_{x=0} = 0 \tag{47}$$

$$\rho'_1 - \left.\frac{p'_1}{\bar{c}_1^2}\right|_{x=0} = 0 \tag{48}$$

Because of the convective nature of the vorticity and entropy waves, their distributions at the outlet must be determined as a part of the solution. Finally, the pressure at both the inlet and outlet are specified to be acoustically open:

$$p'_1|_{x=0} = 0 \quad \text{and} \quad p'_2|_{x=L} = 0 \tag{49}$$

D. System Equations

For each domain, $N_x + 1$, $N_r + 1$, and N_t collocation points are defined in the axial, radial, and circumferential directions, respectively:

$$x_i = \cos\frac{\pi i}{N_x}, \qquad i = 0, \ldots, N_x \tag{50}$$

$$r_i = \cos\frac{\pi i}{N_r}, \qquad i = 0, \ldots, N_r \tag{51}$$

$$\theta_i = \frac{2\pi i}{N}, \qquad i = 1, \ldots, N_t \tag{52}$$

With appropriate specifications of boundary conditions at the inlet, outlet, and wall, as well as the jump conditions across the flame, Eqs. (17–21) can be combined and written as

$$\underbrace{\begin{pmatrix}\boldsymbol{\zeta}_1 & \boldsymbol{\zeta}_3\\ \boldsymbol{\zeta}_4 & \boldsymbol{\zeta}_2\end{pmatrix}}_{X}\begin{pmatrix}\boldsymbol{\xi}_1\\ \boldsymbol{\xi}_2\end{pmatrix} = 0 \tag{53}$$

Here, $\boldsymbol{\zeta}_1, \boldsymbol{\zeta}_2, \boldsymbol{\zeta}_3$, and $\boldsymbol{\zeta}_4$ are submatrices of dimension $[5(N+1)]^2$ with $N = (N_x + 1)(N_r + 1)N_t \cdot 1$. The column vectors $\boldsymbol{\xi}_1$ and $\boldsymbol{\xi}_2$ of length $5(N+1)$ contain unknowns ρ, u_x, u_r, u_θ, and p. Equation (53) admits a nontrivial solution only when the determinant of the matrix vanishes:

$$\begin{vmatrix}\boldsymbol{\zeta}_1 & \boldsymbol{\zeta}_3\\ \boldsymbol{\zeta}_4 & \boldsymbol{\zeta}_2\end{vmatrix} = 0 \tag{54}$$

The solution to the preceding system yields the complex frequency Ω of the oscillating field. Once this quantity is determined, the spatial distributions in the flowfield can be obtained from Eq. (53).

The matrix X becomes very large in the presence of spatially nonuniform flowfields, which complicates the numerical solution of Eq. (54). Classical methods such as Newton–Raphson iteration can be employed, but the results are sensitive to the initialization data. Furthermore, it is sometimes challenging to distinguish a genuine physical mode from numerical artifacts. Sun et al. [30] addressed this difficulty by employing an extended form of the integral winding technique [31,32]. It was shown that the method leads to rapidly converged physical solutions and does not exhibit strong sensitivity to initial conditions. The approach will be employed at present.

III. Model Validation

The theoretical formulation and numerical method are validated against analytical solutions for disturbances in a quasi-one-dimensional duct with unsteady heat release proportional to the acoustic velocity [33]. The duct inlet is choked, and the outlet is open. The corresponding conditions are, respectively,

$$\frac{\rho'}{\bar{\rho}_1} + \frac{u'_x}{\bar{u}_{x1}} = 0, \qquad x = 0 \tag{55}$$

$$p' = 0, \qquad x = l \tag{56}$$

where l is the duct length. The inlet stagnation temperature T_{01} is held constant and spatially uniform at 288 K, and the pressure is 10^5 Pa. Heat release occurs at the middle of the duct with a temperature ratio T_{02}/T_{01} of 6. Two different forms of heat release are considered here:

$$\dot{Q}'(t) = 0 \tag{57}$$

$$\dot{Q}'(t) = C_p(\bar{T}_{02} - \bar{T}_{01})(\bar{\rho}_1 u'_{x1} + \rho'_1\bar{u}_{x1}) \tag{58}$$

Downloaded by GEORGIA INST OF TECHNOLOGY on March 24, 2017 | http://arc.aiaa.org | DOI: 10.2514/1.B36055

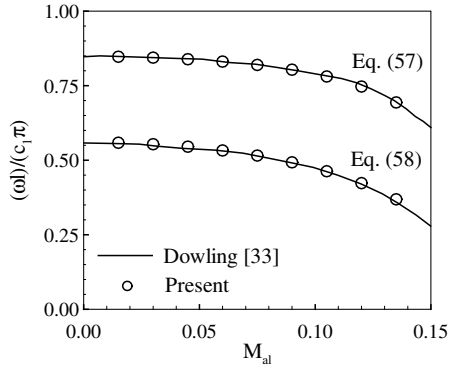

Fig. 3 Lowest frequency of oscillation as a function of inlet Mach number.

Figure 3 shows the calculated lowest frequencies of oscillation using the unsteady heat release described by Eqs. (57) and (58). Excellent agreement with the results given in [33] is observed.

The present theoretical approach is capable of reproducing results from well-studied model problems; the treatment of the jump conditions across the flame appears to be correct.

IV. Effect of Circumferentially Nonuniform Heat Release

With the underlying model validated, we come to the main problem of instability in a cylindrical combustion chamber with a circumferentially nonuniform heat source. As an example, the classical $n-\tau$ model [34,35] is employed to model unsteady heat release. In this formulation, the fluctuations in heat release are taken as linearly proportional to the fluctuating velocity, with a time delay introduced:

$$\frac{\dot{Q}'(t)}{\bar{\dot{Q}}} = n\frac{u_x'(t-\tau)}{\bar{c}} \quad \text{or} \quad \dot{Q}'(t) = n\frac{\bar{\dot{Q}}}{\bar{c}}u_x'(t-\tau) \tag{59}$$

Table 1 Nomenclature for case studies

Case	Description
1	Spatially uniform $\dot{Q}$
2	Circumferentially distributed $\bar{\dot{Q}}$ with azimuthally nonuniform flowfield downstream of flame
3	Circumferentially distributed $\dot{Q}$ with uniform flowfield downstream of flame

Table 2 Example parameters

Example	M_1	l_1, m	k	τ, ms	ω	α
1	0.05	0.6	4	1.5	824.7	12.4
2	0.1	0.6	3	1.5	753.6	11.6
3	0.1	0.6	4	2.0	786.7	9.52
4	0.1	0.5	4	1.0	873.2	7.06

Table 3 Grid independence study for example 3, $\sigma = 2$

N_x	N_θ	Ω
25	07	$781.8 + i1.463$
25	15	$781.5 + i1.330$
25	21	$781.5 + i1.329$
25	25	$781.5 + i1.329$
21	25	$781.5 + i1.329$
17	25	$781.5 + i1.329$

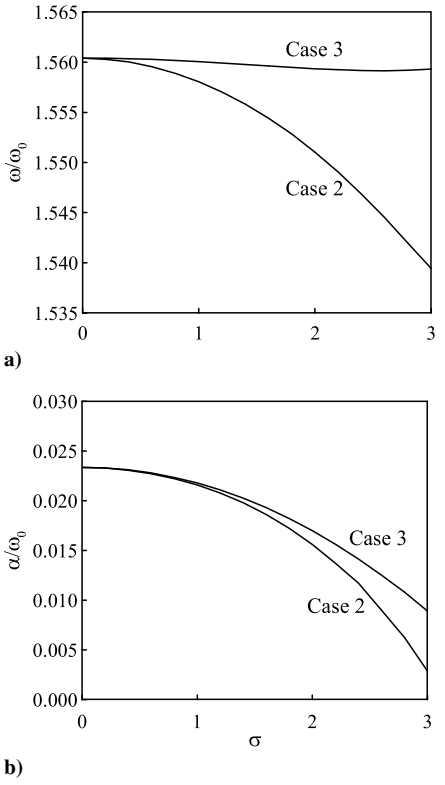

Fig. 4 Representations of a) lowest frequency, and b) associated growth rate as a function of σ (example 1: $M_1 = 0.05$, $k = 4$, $l_1 = 0.6$, and $\tau = 1.5$ ms).

The preceding equation indicates three possible sources of nonuniformity in the fluctuating rate of heat release: the mean rate of heat release, the interaction index n, and the time delay τ. The first two effects are essentially the same because they both act as proportionality constants for the unsteady velocity disturbance. Without loss of generality, we may subsume n within $\dot{Q}$ because only the overall magnitude of the combustion response gain is of interest at present. This approach is based on the theoretical formulation in the previous sections. The effect of time delay will be investigated separately.

Appealing to the linearized unsteady heat-release model given by Eq. (59), and postulating a time delay between velocity and heat-release fluctuations, we may write

$$\dot{Q}'(t) = C_p(\bar{T}_{02} - \bar{T}_{01})\bar{\rho}_1 u_{x1}'(t-\tau) \tag{60}$$

Setting $\bar{T}_{02} = \bar{T}_{01}(k + \sigma \sin\theta)$, where k is the stagnation temperature ratio and σ is the degree of the nonuniformity, we have

$$\dot{Q}'(\theta, t) = C_p(k - 1 + \sigma \sin\theta)\bar{T}_{01}\bar{\rho}_1\hat{u}_{x1}e^{-i\Omega\tau} \tag{61}$$

With a uniform τ, this equation allows us to study the effect of spatial distribution of the combustion response gain. Likewise, we may set $\bar{T}_{02} = k\bar{T}_{01}$ and $\tau = \tau_0(1 + \sigma \sin\theta)$, where τ_0 is a reference time delay, to obtain

$$\dot{Q}'(\theta, t) = C_p(k-1)\bar{T}_{01}\bar{\rho}_1\hat{u}_{x1}e^{-i\Omega\tau_0(1+\sigma \sin\theta)} \tag{62}$$

This form allows us to study the effect of spatial distribution of the combustion response time delay with a spatially uniform gain. In both cases, σ is used unambiguously to refer to the degree of the nonuniformity.

For the nonuniformity in unsteady heat release modeled by Eq. (61), we shall also consider the effect of what will be referred to as thermal redistribution. Given the circumferential nonuniformity in heat-release gain, the temperature distribution downstream of the flame will be nonuniform. In general, due to mixing and heat conduction processes, there will be some axial length over which the

Downloaded by GEORGIA INST OF TECHNOLOGY on March 24, 2017 | http://arc.aiaa.org | DOI: 10.2514/1.B36055

Downloaded by GEORGIA INST OF TECHNOLOGY on March 24, 2017 | http://arc.aiaa.org | DOI: 10.2514/1.B36055

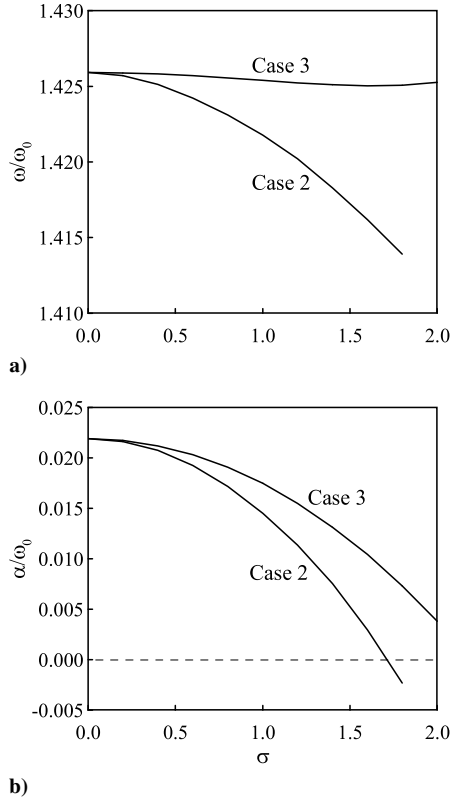

Fig. 5 Representations of a) lowest frequency, and b) associated growth rate as a function of σ (example 2: $M_1 = 0.1$, $k = 3$, $l_1 = 0.6$, and $\tau = 1.5$ ms).

temperature distribution will relax and become spatially uniform. We consider two different situations in which 1) the temperature distribution downstream of the flame is azimuthally nonuniform, and

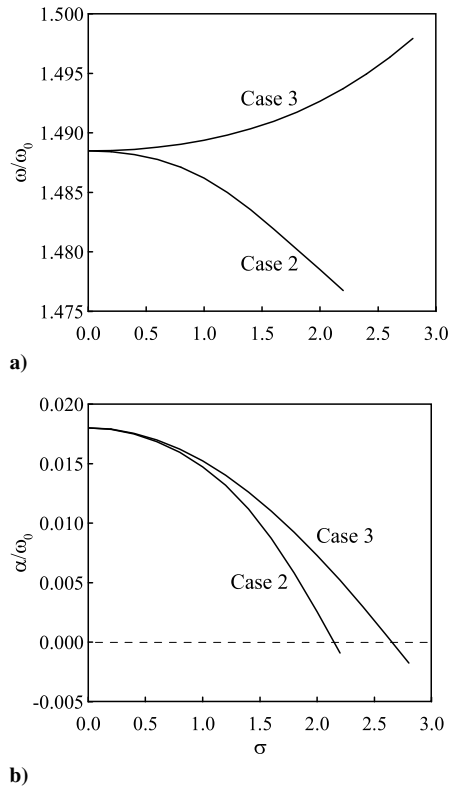

Fig. 6 Representations of a) lowest frequency, and b) associated growth rate as a function of σ (example 3: $M_1 = 0.1$, $k = 4$, $l_1 = 0.6$, and $\tau = 2$ ms).

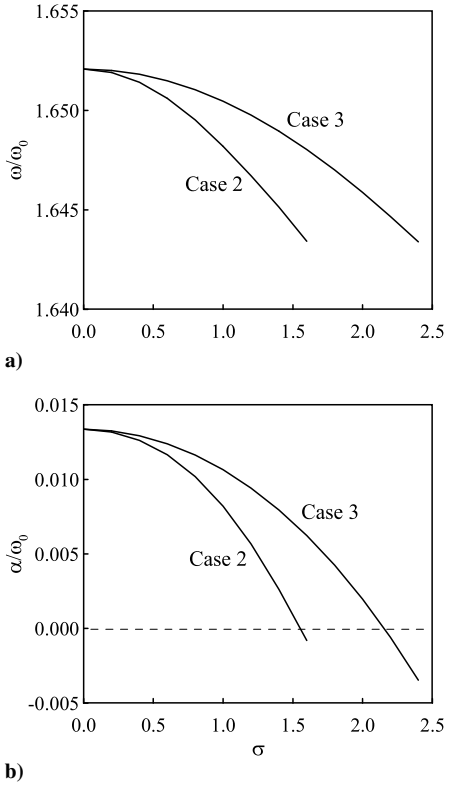

Fig. 7 Representations of a) lowest frequency, and b) associated growth rate as a function of σ (example 4: $M_1 = 0.1$, $k = 4$, $l_1 = 0.5$, and $\tau = 1$ ms).

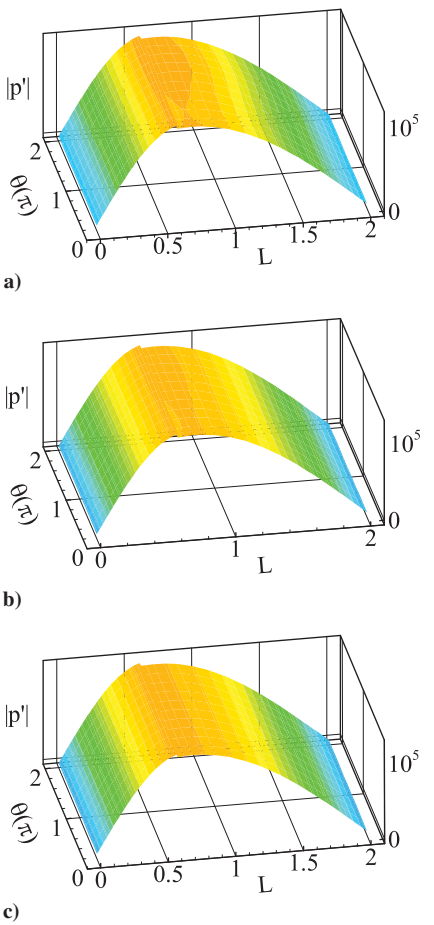

Fig. 8 Distributions of pressure fluctuation amplitude (arbitrary scale) along axial and circumferential directions for a) case 1, b) case 2, and c) case 3 (example 3: $M_1 = 0.1$, $k = 4$, $l_1 = 0.6$, and $\tau = 2$ ms).

Downloaded by GEORGIA INST OF TECHNOLOGY on March 24, 2017 | http://arc.aiaa.org | DOI: 10.2514/1.B36055

2) the temperature distribution is azimuthally uniform at every axial location. The two cases represent respectively the extremes where the characteristic time for turbulent mixing is much longer and much shorter than the flow residence time. For comparison, we also consider the case in which the combustion, and hence postflame temperature, is circumferentially uniform. Table 1 summarizes the cases.

We first investigate the baseline case, in which the gain and time delay of the heat-release response are uniform. The results for several different combinations of Mach number M_1, length of zone 1 (l_1), stagnation temperature ratio k, and heat-release time delay τ are shown in Table 2. The upstream stagnation temperature remains fixed at 288 K. The growth rates for all combinations are positive, indicating that the system is unstable.

Grid independence studies were performed by varying the number of grid points in the axial and circumferential directions, N_x and N_θ. The results of one such study with $\sigma = 2$ are shown in Table 3. Convergence is rapidly achieved for the geometry and boundary conditions under consideration.

A. Results for Nonuniform Heat-Release Gain

The effect of nonuniform heat-release gain is investigated by performing a parameter sweep over the nonuniformity strength σ for cases 1 and 2. Figure 4 shows the lowest frequency and growth rate as a function of σ for example 1 in Table 2. The results are nondimensionalized using $\omega_0 = 528.5$ Hz, the frequency found for $M_1 = 0.1$, $k = 1$, and $\tau = 0$. As σ is increased in the two cases, the frequencies decrease slightly, and the growth rates begin positive and tend toward zero. The system is always unstable because the growth rates remain positive. To maintain a realistic situation, the value of σ must be in the interval $[0, k-1]$, or the downstream temperature becomes lower than its upstream counterpart. Figure 5 shows the lowest frequency and growth rate for example 2. In the range of σ considered, the growth rate changes sign for case 1 but not for case 2. Figures 6 and 7 show similar plots for examples 3 and 4, respectively. In both figures, the growth rates for cases 2 and 3 become negative, but the slope is steeper in Fig. 7.

The results in Figs. 4–7 indicate that, as σ increases, the frequency of oscillation remains largely unchanged, whereas the growth rates decrease. This knowledge may be applicable in the design of combustors, for the attenuation of potentially deleterious acoustic waves.

For a given frequency, the distributions of the amplitudes of perturbation quantities can be obtained by solving the linearized equations of motion as described in Sec. III.D. Figure 8a shows the distributions of pressure fluctuation along the axial and circumferential directions for case 1. The pressure fluctuation amplitude is azimuthally uniform. Figures 8b and 8c show the fluctuating pressure amplitudes for cases 2 and 3, respectively, where $\sigma = 1.0$. The pressure fluctuations show only slight variations in the circumferential direction near the heat source, indicating that nonuniformity has little effect on acoustic pressure fluctuations.

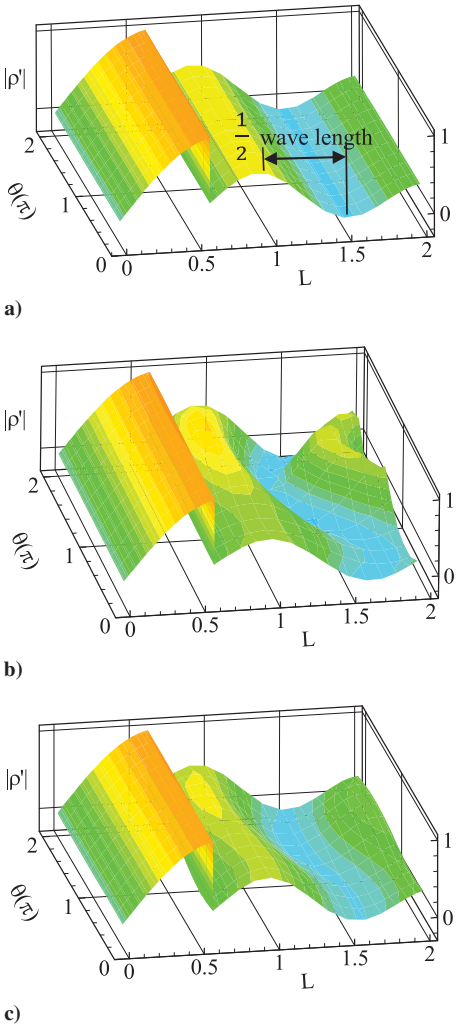

Fig. 9 Distributions of density fluctuation amplitude (arbitrary scale) along axial and circumferential directions for a) case 1, b) case 2, and c) case 3 (example 3: $M_1 = 0.1$, $k = 4$, $l_1 = 0.6$, and $\tau = 2$ ms).

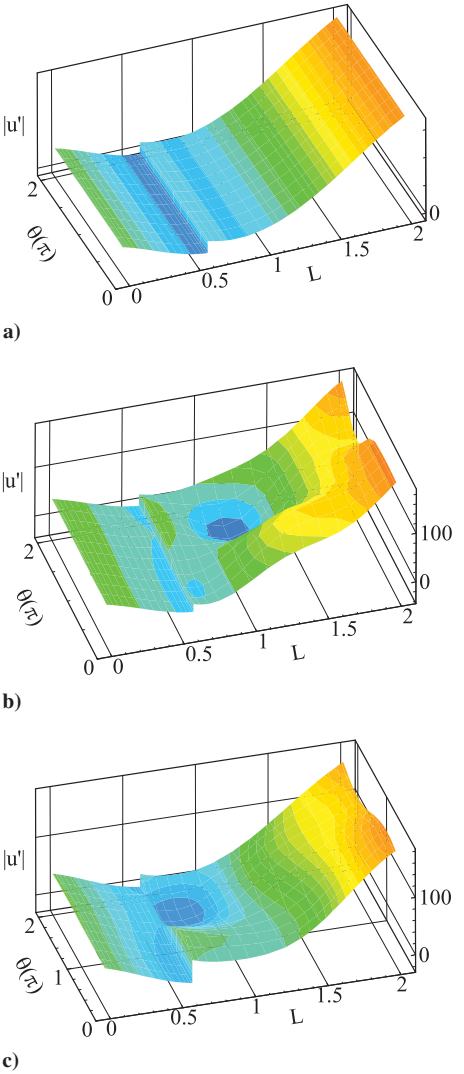

Fig. 10 Distributions of velocity fluctuation amplitude (arbitrary scale) along axial and circumferential directions for a) uniform case, b) case 2, and c) case 1 (example 3: $M_1 = 0.1$, $k = 4$, $l_1 = 0.6$, and $\tau = 2$ ms).

Downloaded by GEORGIA INST OF TECHNOLOGY on March 24, 2017 | http://arc.aiaa.org | DOI: 10.2514/1.B36055

Figure 9 shows density fluctuation distributions for the three cases. The density fluctuation can be decomposed into

$$\rho' = \rho'_s + \rho'_a \tag{63}$$

where ρ_s and ρ_a denote the entropic and acoustic components, respectively. The entropy wavelength can be estimated by $2\pi u_x/\omega$. Here, the mean flow velocity is 141 m/s, and ω is 786 s^{-1}. With these values, the entropy wavelength is about 1.1 m, which corresponds to the wavelength scale observed in Fig. 9a. Thus, the entropy wave dominates the density fluctuation in the region downstream of the heat source. Figure 9b shows that the density fluctuation amplitude varies in the circumferential direction because of the circumferential nonuniformity of the temperature and entropy wave strength.

Figure 10 shows the distributions of the axial velocity fluctuation for all three cases. For case 1, the axial velocity fluctuation is uniformly distributed in the circumferential direction. The velocity fluctuation can be decomposed into

$$u' = u'_v + u'_p \tag{64}$$

where u_v and u_a denote the vortical and acoustic contribution, respectively. The results in Fig. 10a show that there are no vortical waves present in the case of a circumferentially uniform heat source. Figure 10b indicates the dominance of the acoustic part in the axial velocity fluctuation, but with a small-scale disturbance superimposed on it and convected by the flow. The small-scale wavelength may be identified with that of the entropy wave. A vortical wave is again present in Fig. 10c, but this wave is slightly different from that in Fig. 10b. In this case, vortical, acoustic, and entropy waves are all coupled downstream of the flame. Starting from the conservation

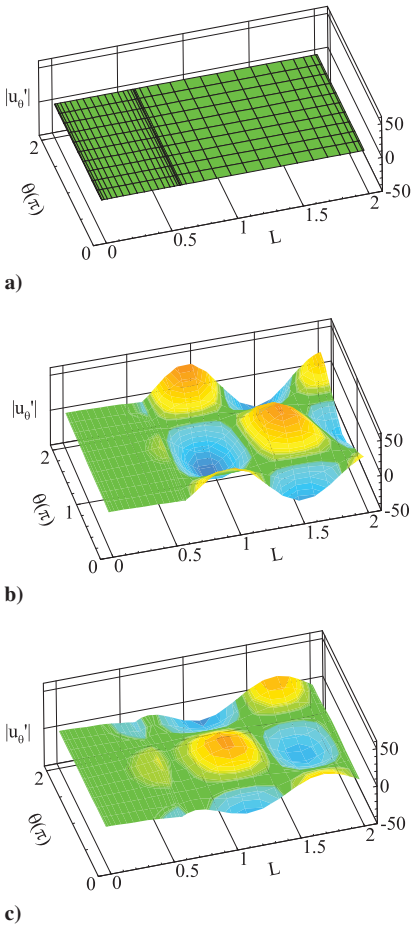

Fig. 11 Distributions of circumferential velocity fluctuation amplitude (arbitrary scale) along axial and circumferential directions for a) case 1, b) case 2, and c) case 3.

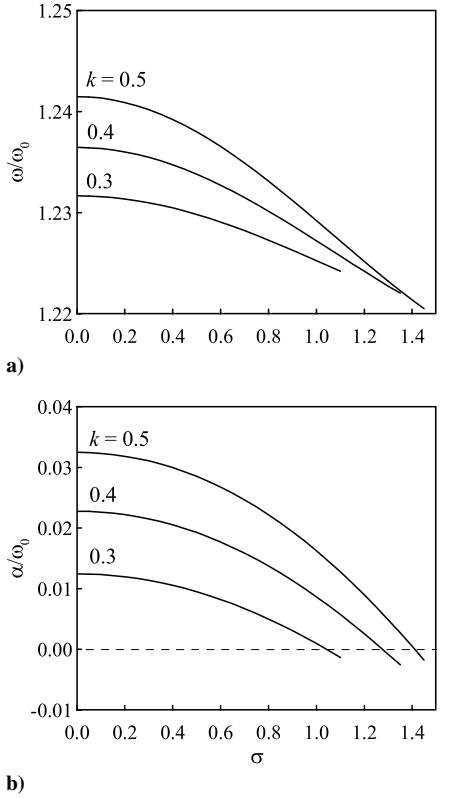

Fig. 12 Representations of a) lowest frequency, and b) associated growth rate as a function of σ for $M_1 = 0.05$, $k = 2$, $l_1 = 0.6$, and $\tau_0 = 2$ ms.

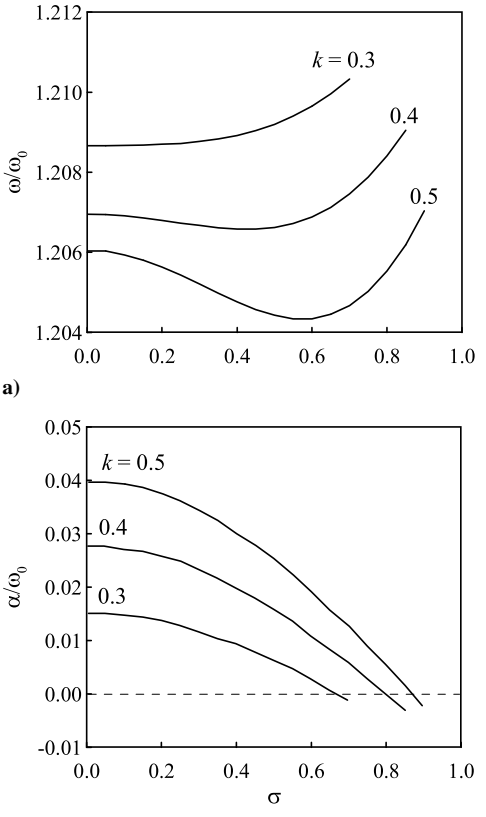

Fig. 13 Representations of a) lowest frequency, and b) associated growth rate as a function of σ for $M_1 = 0.05$, $k = 2$, $l_1 = 0.6$, and $\tau_0 = 3$ ms.

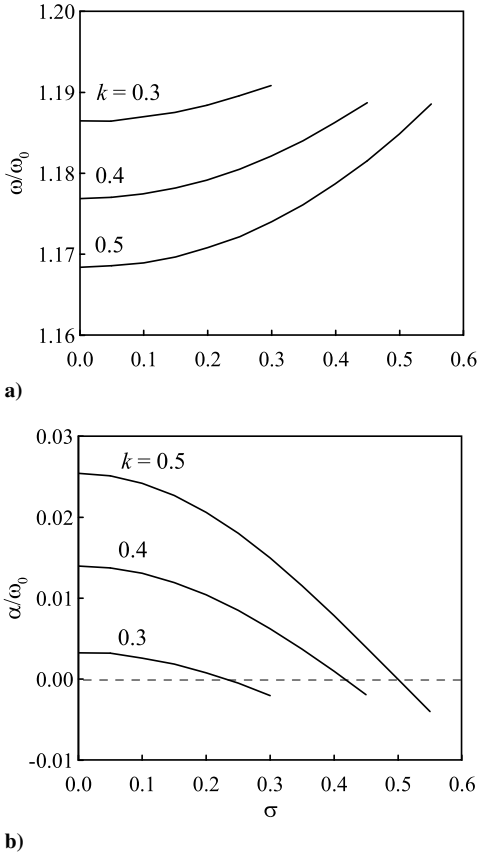

Fig. 14 Representations of a) lowest frequency, and b) associated growth rate as a function of σ for $M_1 = 0.05$, $k = 2$, $l_1 = 0.6$, and $\tau_0 = 4$ ms.

equations, one can show that the vortical velocity may be determined from

$$\frac{\partial u'_{xv}}{\partial x} + \frac{1}{R}\frac{\partial u'_{\theta v}}{\partial \theta} = 0 \tag{65}$$

Figure 11 confirms that the circumferential component of the vortical velocity is nonzero if the axial component of the vortical velocity is nonzero. For case 1 shown in Fig. 11a, the circumferential velocity is zero because no vortical waves exist, whereas in the other two cases, there are evidently vortical waves present.

B. Results for Nonuniform Heat-Release Time Delay

The effect of circumferential distribution of heat-release time delay is examined, while holding the gain fixed, as per Eq. (59). Here, $k = 2$, $l_1 = 0.6$, the inlet flow velocity Mach number is 0.05, and the other flow parameters are the same as those in Sec. IV.A. The oscillation frequency and growth rate are again obtained by performing a parameter sweep over the nonuniformity strength σ.

Figure 12–14 show the lowest frequency and corresponding growth rate as a function of σ, with different values of k and τ_0. For time delays of 2, 3, and 4 ms with a uniform heat source, the growth rates are positive, and the system is unstable. The growth rate reaches its maximum value when $\tau_0 = 3$ ms. The growth rate decreases as σ increases for each τ_0, but the lowest frequency changes marginally. At some critical value of σ, the growth rate changes sign, indicating that the system becomes stable.

V. Conclusions

A theoretical model based on the inviscid-flow equations of motion has been developed to predict the linear behaviors of thermoacoustic instabilities in a Rijke tube excited by a planar, circumferentially nonuniform heat source. A spectral collocation method was used to solve the formulation, with a domain decomposition method used to accommodate discontinuities across the flame zone. The effects of circumferential distributions of the combustion response gain and time delay were investigated separately. Results indicate that both distributions play important roles in determining the stability characteristics of the system. As the extent of the nonuniformity increases, the growth rate decreases, in some cases significantly enough to change sign. A nonuniform azimuthal distribution of combustion response parameters may provide a stabilizing effect. Moreover, interactions between acoustic waves and the nonuniform heat source produce vortical waves, often neglected in combustion instability analyses, which may have a significant effect on the system stability.

Appendix: LEE Coefficients

$$A_1 = -i\Omega + \frac{\partial \bar{u}_x}{\partial x}; \qquad A_2 = \bar{u}_x; \qquad A_3 = \bar{\rho} \tag{A1}$$

$$A_4 = \frac{\bar{\rho}}{(r+1)}; \qquad A_5 = \bar{\rho} \tag{A2}$$

$$A_6 = \frac{\bar{\rho}}{(r+1)} + \frac{\partial \bar{\rho}}{\partial r}; \qquad A_7 = \frac{1}{(r+1)}\frac{\partial \bar{\rho}}{\partial \theta}; \qquad A_8 = \frac{\partial \bar{\rho}}{\partial x} \tag{A3}$$

$$B_1 = -i\Omega\bar{\rho}; \qquad B_2 = \bar{\rho}\bar{u}_x; \qquad B_3 = 1 \tag{A4}$$

$$C_1 = -i\Omega\bar{\rho}; \qquad C_2 = \bar{\rho}\bar{u}_x; \qquad C_3 = \frac{1}{(r+1)} \tag{A5}$$

$$D_1 = \bar{u}_x\frac{\partial \bar{u}_x}{\partial x}; \qquad D_2 = -i\Omega\bar{\rho} + \bar{\rho}\frac{\partial \bar{u}_x}{\partial x} \tag{A6}$$

$$D_3 = \bar{\rho}\bar{u}_x; \qquad D_4 = \bar{\rho}\frac{\partial \bar{u}_x}{\partial r} \tag{A7}$$

$$D_5 = \frac{\bar{\rho}}{(r+1)}\frac{\partial \bar{u}_x}{\partial \theta}; \qquad D_6 = 1 \tag{A8}$$

$$E_1 = i\Omega + \frac{\bar{u}_x}{\bar{\rho}}\frac{\partial \bar{\rho}}{\partial x}; \qquad E_2 = -\bar{u}_x \tag{A9}$$

$$E_3 = \frac{1}{\bar{c}^2}\frac{\partial \bar{p}}{\partial r} - \frac{\partial \bar{\rho}}{\partial r} \tag{A10}$$

$$E_4 = \left(\frac{1}{\bar{c}^2}\frac{\partial \bar{p}}{\partial \theta} - \frac{\partial \bar{\rho}}{\partial \theta}\right)\frac{1}{(r+1)} \tag{A11}$$

$$E_5 = \frac{1}{\bar{c}^2}\frac{\partial \bar{p}}{\partial x} - \frac{\partial \bar{\rho}}{\partial x} \tag{A12}$$

$$E_6 = -i\Omega\frac{1}{\bar{c}^2} - \frac{\gamma\bar{u}_x}{\bar{c}^2\bar{\rho}}\frac{\partial \bar{\rho}}{\partial x} \tag{A13}$$

$$E_7 = \frac{\bar{u}_x}{\bar{c}^2} \tag{A14}$$

Downloaded by GEORGIA INST OF TECHNOLOGY on March 24, 2017 | http://arc.aiaa.org | DOI: 10.2514/1.B36055

Downloaded by GEORGIA INST OF TECHNOLOGY on March 24, 2017 | http://arc.aiaa.org | DOI: 10.2514/1.B36055

Acknowledgments

This work was supported in part by the National Natural Science Foundation of China (grant numbers 51206006), the 973 Program (grant number 2012CB720200), and in part by the William R. T. Oakes Endowment of the Georgia Institute of Technology.

References

[1] De Luca, L., Price, E. W., and Summerfield, M., *Nonsteady Burning and Combustion Stability of Solid Propellants*, Vol. 143, Progress in Astronautics and Aeronautics, AIAA, Washington, D.C., 1992.

[2] Yang, V., Brill, T. B., and Ren, W., *Solid Propellant Chemistry Combustion and Motor Interior Ballistics*, Vol. 185, Progress in Astronautics and Aeronautics, AIAA, Reston, VA, 2000.

[3] Harrje, D. T., and Reardon, F. H., "Liquid Propellant Rocket Combustion Instability," NASA Special Publ. 194, 1972.

[4] Anderson, W. E., and Yang, V., *Liquid Rocket Engine Combustion Instability*, Vol. 169, Progress in Astronautics and Aeronautics, AIAA, Washington, D.C., 1995.

[5] Dranovsky, M. L., Yang, V., Culick, F. E. C., and Talley, D. G., *Combustion Instabilities in Liquid Rocket Engines: Testing and Development Practices in Russia*, Vol. 221, Progress in Astronautics and Aeronautics, AIAA, Reston, VA, 2007.

[6] Yang, V., and Culick, F. E. C., "Analysis of Low Frequency Combustion Instabilities in a Laboratory Ramjet Combustor," *Combustion Science and Technology*, Vol. 45, Nos. 1–2, 1986, pp. 1–25. doi:10.1080/00102208608923839

[7] Choi, J.-Y., Ma, F., and Yang, V., "Combustion Oscillations in a Scramjet Engine Combustor with Transverse Fuel Injection," *Proceedings of the Combustion Institute*, Vol. 30, No. 2, 2005, pp. 2851–2858.

[8] Lin, K.-C., Jackson, K., Behdadnia, R., Jackson, T. A., Ma, F., and Yang, V., "Acoustic Characterization of an Ethylene-Fueled Scramjet Combustor with a Cavity Flameholder," *Journal of Propulsion and Power*, Vol. 26, No. 6, 2010, pp. 1161–1170. doi:10.2514/1.43338

[9] Sung, H. G., and Yang, V., "A Unified Analysis of the Internal Flowfield in an Integrated Rocket-Ramjet Engine 2: Ramjet Sustainer," *Journal of Aerospace Engineering*, Vol. 27, No. 2, 2014, pp. 398–403. doi:10.1061/(ASCE)AS.1943-5525.0000256

[10] Dowling, A. P., and Stow, S. R., "Acoustic Analysis of Gas Turbine Combustors," *Journal of Propulsion and Power*, Vol. 19, No. 5, 2003, pp. 751–764. doi:10.2514/2.6192

[11] Lieuwen, T. C., and Yang, V., *Combustion Instabilities in Gas Turbine Engines: Operational Experience, Fundamental Mechanisms and Modeling*, Vol. 210, Progress in Astronautics and Aeronautics, AIAA, Reston, VA, 2005.

[12] Culick, F. E. C., "Stability of Three-Dimensional Motions in a Combustion Chamber," *Combustion Science and Technology*, Vol. 10, Nos. 3–4, 1975, pp. 109–124. doi:10.1080/00102207508946663

[13] Culick, F. E. C., "Nonlinear Behavior of Acoustic Waves in Combustion Chambers—1," *Acta Astronautica*, Vol. 3, Nos. 9–10, 1976, pp. 715–734. doi:10.1016/0094-5765(76)90107-7

[14] Culick, F. E. C., and Yang, V., "Prediction of the Stability of Unsteady Motions in Solid-Propellant Rocket Motors," *Nonsteady Burning and Combustion Stability of Solid Propellants*, edited by De Luca, L. P., Price, E. W., and Summerfield, M., Vol. 143, AIAA, Washington, D.C., 1992, pp. 719–779.

[15] Culick, F. E. C., and Yang, V., "Overview of Combustion Instabilities in Liquid-Propellant Rocket Engines," *Liquid Rocket Engine Combustion Instability*, edited by Anderson, W. E., and Yang, V., Vol. 169, Progress in Astronautics and Aeronautics, AIAA, Washington, D.C., 1995, pp. 3–37.

[16] Yang, V., Kim, S. I., and Culick, F. E. C., "Triggering of Longitudinal Pressure Oscillations in Combustion Chambers. 1: Nonlinear Gasdynamics," *Combustion Science and Technology*, Vol. 72, Nos. 4–6, 1990, pp. 183–214. doi:10.1080/00102209008951647

[17] Wicker, J. M., Greene, W. D., Kim, S.-I., and Yang, V., "Triggering of Longitudinal Combustion Instabilities in Rocket Motors: Nonlinear Combustion Response," *Journal of Propulsion and Power*, Vol. 12, No. 6, 1996, pp. 1148–1158. doi:10.2514/3.24155

[18] Flandro, G. A., Fischbach, S. R., and Majdalani, J., "Nonlinear Rocket Motor Stability Prediction: Limit Amplitude, Triggering, and Mean Pressure Shift," *Physics of Fluids*, Vol. 19, Sept. 2007, Paper 094101.

[19] Rayleigh, J. W. S., *The Theory of Sound*, Vol. 1, McMillan, New York, 1945.

[20] Culick, F. E. C., "A Note on Rayleigh's Criterion," *Combustion Science and Technology*, Vol. 56, Nos. 4–6, 1987, pp. 159–166. doi:10.1080/00102208708947087

[21] Ffowcs-Williams, J. E., and Howe, M. S., "The Generation of Sound by Density Inhomogeneities in Low Mach Number Nozzle Flows," *Journal of Fluid Mechanics*, Vol. 70, No. 3, 1975, pp. 605–622. doi:10.1017/S0022112075002224

[22] Marble, F. E., and Candel, S. M., "Acoustic Disturbance from Gas Non-Uniformities Convected Through a Nozzle," *Journal of Sound and Vibration*, Vol. 55, No. 2, 1977, pp. 225–243. doi:10.1016/0022-460X(77)90596-X

[23] Polifke, W., Paschereit, C. O., and Döbbeling, K., "Constructive and Destructive Interference of Acoustic and Entropy Waves in a Premixed Combustor with a Choked Exit," *International Journal of Acoustics and Vibration*, Vol. 6, No. 3, 2001, pp. 135–146.

[24] Motheau, E., Nicoud, F., and Poinsot, T., "Mixed Acoustic–Entropy Combustion Instabilities in Gas Turbines," *Journal of Fluid Mechanics*, Vol. 749, June 2014, pp. 542–576. doi:10.1017/jfm.2014.245

[25] Dowling, A. P., and Mahmoudi, Y., "Combustion Noise," *Proceedings of the Combustion Institute*, Vol. 35, No. 1, 2015, pp. 65–100. doi:10.1016/j.proci.2014.08.016

[26] Li, L., and Sun, X., "Effect of Vorticity Waves on Azimuthal Instabilities in Annular Chambers," *Combustion and Flame*, Vol. 162, No. 3, 2015, pp. 628–641. doi:10.1016/j.combustflame.2014.09.011

[27] Acharya, V., and Lieuwen, T. C., "Response of Non-Axisymmetric Premixed, Swirl Flames to Helical Disturbances," *Proceedings of the ASME Turbo Expo 2014: Turbine Technical Conference and Exposition*, American Soc. of Mechanical Engineers Paper GT2014-27059, New York, 2014.

[28] Li, L., Yang, L., and Sun, X., "Effect of Distributed Heat Source on Low Frequency Thermoacoustic Instabilities," *Journal of Sound and Vibration*, Vol. 332, No. 12, 2013, pp. 3098–3111. doi:10.1016/j.jsv.2013.01.011

[29] Heinrichs, W., "Spectral Collocation Schemes on the Unit Disc," *Journal of Computational Physics*, Vol. 199, No. 1, 2004, pp. 66–86. doi:10.1016/j.jcp.2004.02.001

[30] Sun, X., Sun, D., and Yu, W., "A Model to Predict Stall Inception of Transonic Axial Flow Fan/Compressors," *Chinese Journal of Aeronautics*, Vol. 24, No. 6, 2011, pp. 687–700. doi:10.1016/S1000-9361(11)60081-2

[31] Brazier-Smith, P. R., and Scott, J. F. M., "On the Determination of the Roots of Dispersion Equations by Use of Winding Number Integrals," *Journal of Sound and Vibration*, Vol. 145, No. 3, 1991, pp. 503–510. doi:10.1016/0022-460X(91)90119-5

[32] Ivansson, S., and Karasalo, I., "Computation of Modal Wavenumbers Using an Adaptive Winding-Number Integral Method with Error Control," *Journal of Sound and Vibration*, Vol. 161, No. 1, 1993, pp. 173–180. doi:10.1016/0022-460X(93)90410-D

[33] Dowling, A. P., "The Calculation of Thermoacoustic Oscillations," *Journal of Sound and Vibration*, Vol. 180, No. 4, 1995, pp. 557–581. doi:10.1006/jsvi.1995.0100

[34] Lang, W., Poinsot, T., and Candel, S. M., "Active Control of Combustion Instability," *Combustion and Flame*, Vol. 70, No. 3, 1987, pp. 281–289. doi:10.1016/0010-2180(87)90109-X

[35] McManus, K. R., Poinsot, T., and Candel, S. M., "A Review of Active Control of Combustion Instabilities," *Progress in Energy and Combustion Science*, Vol. 19, No. 1, 1993, pp. 1–29. doi:10.1016/0360-1285(93)90020-F

J. C. Oefelein
Associate Editor